

## Microstructure and microsegregation in directionally solidified Ti–46Al–8Nb alloy

LIU Guo-huai, LI Xin-zhong, SU Yan-qing, CHEN Rui-run, GUO Jing-jie, FU Heng-zhi

School of Materials Science and Engineering, Harbin Institute of Technology, Harbin 150001, China

Received 9 September 2011; accepted 6 January 2012

**Abstract:** Directional solidification experiments were conducted for Ti–46Al–8Nb alloy at the growth rates ranging from 3 to 70  $\mu\text{m/s}$ . The microstructure evolution and microsegregation pattern were investigated. In the range of growth rate, a regular dendritic structure appears and the primary dendrite spacing decreases with increasing growth rate. The peritectic reaction is observed during the solidification and the final microstructure is composed of  $\alpha_2/\gamma$  lamellar structure and retained  $\beta(B2)$  after directional solidification. The lamellar orientation is found to be parallel and  $45^\circ$  to the primary growth direction of  $\beta$  dendrite. Peritectic reaction leads to significant chemical inhomogeneity, in which aluminum is rich in interdendritic liquid and niobium is rich in the core of  $\beta$  dendrite during the solidification. With the nucleation and growth of  $\alpha$  phase, the segregation amplitude of niobium increases, which promotes the formation of  $B2$  phase, while aluminum rich in the interdendritic becomes homogeneous gradually.

**Key words:** Ti–46Al–8Nb alloy; directional solidification; microstructure evolution; microsegregation; lamellar orientation

### 1 Introduction

TiAl-based alloys are considered to be attractive candidate materials for high temperature structural applications due to their excellent low density, high specific modulus and creep resistance [1–6]. Alloying element Nb is added to improve high temperature resistance, lamellar structure stability and oxidation resistance [7,8]. Ti–46Al–8Nb (mole fraction, %) intermetallic alloy developed within the pan-European IMPRESS project is one of the advanced materials for turbines of aircraft engines and gas-burning power-generation plants due to its lightweight and creep resistant to high temperature (800 °C) [9,10]. In order to successfully and effectively achieve the industry application, detailed information about microstructure formation and evolution during directional solidification (DS) of TiAlNb alloys is needed. However, up to now, there is limited understanding of microstructure development about the TiAlNb alloys. On one side, it can be attributed to the complex solidification path and also subsequent solid-state transformation in the alloys. High Nb addition changes the Ti–Al phase diagram, leading to

the solidification behavior different from binary TiAl alloy [11,12]. On the other side, titanium melt with high activity reacts with all commercially known ceramic crucible materials, which complicates the DS processing significantly.

Nb addition leads to stabilization of the  $\beta$  phase at lower temperature, which, as the ordered  $B2$  phase, could greatly affect the mechanical properties of the alloys. The elongated  $B2$  particles formed by  $\beta$ -stabilizer centralization in interdendritic liquid have been observed in directionally solidified Ti–46Al–8Nb alloys [13]. ZOLLINGER et al [14] have shown that the appearance of  $\alpha$  phase due to the solute segregation leads to coarse retained  $B2$  phase in rapid solidification of Ti–46Al–8Nb alloys. For the clarity, the formation of  $B2$  phase which is connected with the segregation is not yet fully understood up to now. So, it is necessary to investigate the microsegregation and the formation of the  $B2$  phase.

The aim of this study is to determine the microstructure and microsegregation by quenching directionally solidified Ti–46Al–8Nb (mole fraction, %) alloy. The phase transformation path, the detailed microstructure evolution and the microsegregation pattern are investigated at the growth rates ranging from

3 to 70  $\mu\text{m/s}$ . A particular interest is the effect of phase transformation on the segregation of Nb and the formation of  $B2$  phase.

## 2 Experimental

The intermetallic Ti–46Al–8Nb alloy with an actual composition of Ti–46.3Al–7.6Nb (mole fraction, %) was supplied in the form of cast cylindrical ingot, which was fabricated by the induction skull melting (ISM). A bar with 3 mm in diameter and 100 mm in length was cut from the ingot, and placed into the alumina crucible, which had an yttria mould isolating the alloy from the crucible. The Bridgman type apparatus was employed to produce the directionally solidified (DS) bar under the protection of the high-purity argon. After heating to 1790 °C and holding for 30 min, the bar was solidified directionally at the growth rates from 3 to 70  $\mu\text{m/s}$ . After growing to about 35 mm, the sample was quenched into the liquid Ga–In–Sn alloy to restore the solid–liquid interface. The directionally solidified bar was sectioned longitudinally, which was polished using the standard metallographic techniques and etched in a solution of 10 mL HF, 10 mL  $\text{HNO}_3$ , and 180 mL  $\text{H}_2\text{O}$ . The microstructures and the component distribution were examined using a scanning electron microscope (SEM) equipped with an energy dispersive spectrometer (EDS).

## 3 Results and discussion

### 3.1 Microstructure and phase transformation of DS samples

Table 1 gives the various growth conditions applied during directional solidification experiments, as well as the measured primary dendrite arm spacing. The solid–liquid interface has a regular dendritic structure, and the primary dendrite arm spacing gradually decreases with the increase of the growth rate.

**Table 1** Growth conditions used for DS experiments and some measurements of quenching interface

Sample No.	Velocity/ ( $\mu\text{m}\cdot\text{s}^{-1}$ )	Primary dendrite arm spacing/ $10^2\mu\text{m}$	Morphology of interface
1	3	5	Cellular–dendrite
2	5	5	Dendrite
3	15	4.29	Dendrite
4	30	3.33	Dendrite
5	70	3	Dendrite

Figures 1 and 2 show the macrographs of DS samples and microstructures at the growth rates of 3 and

30  $\mu\text{m/s}$ , respectively. Quenching quickly allows freezing in the high temperature phases for subsequent analysis. Microstructure consists of  $\beta$  phase,  $\alpha$  phase,  $\alpha_2/\gamma$  lamellar structure, and  $B2$  phase (ordered  $\beta$  phase). Cubic  $\beta$  phase is easily found to be the primary solidification phase in this alloy by noting that the secondary dendritic arms are orthogonal to the primary arms, as shown in Fig. 1(d) and Fig. 2(d).

According to the TiAlNb equilibrium phase diagram [10], as shown in Fig. 3, an equilibrium solidification of Ti–46Al–8Nb alloy should lead to the following solidification sequence: Liquid  $\rightarrow$  Liquid+ $\beta$  $\rightarrow$  $\beta$  $\rightarrow$  $\beta$ + $\alpha$  $\rightarrow$  $\alpha$  $\rightarrow$  $\alpha$ + $\gamma$  $\rightarrow$  $\alpha_2/\gamma$ + $\gamma$ . However, a mixing zone of liquid,  $\alpha$  and  $\beta$  is observed at the growth rates of 3  $\mu\text{m/s}$  and 30  $\mu\text{m/s}$ , as shown in Figs. 1 and 2. It involves a typical peritectic reaction of  $L+\beta$  $\rightarrow$  $\alpha$  where the peritectic phase  $\alpha$  envelopes the primary phase  $\beta$  firstly by nucleation and then the dissolution of primary  $\beta$  and growth of peritectic  $\alpha$  happen near the trijunction. This suggests that the solidification sequence deviates from the equilibrium process resulting from the solute segregation and the change of the solidification parameters. When the peritectic reaction occurs, the primary  $\beta$  is isolated by peritectic phase  $\alpha$ , and the growth of peritectic phase  $\alpha$  leads to the enrichment of the  $\beta$ -stabilizer in the core of dendrite, which promotes the formation of  $B2$  phase. The white light  $B2$  phase is observed distributed in the core of the dendrite, as shown in Figs. 1(b) and 2(b). The observed  $B2$  phase is maintained  $\beta$  phase. Following by further decrease of temperature, the transformation of  $\alpha$  $\rightarrow$  $\alpha$ + $\gamma$  occurs. The final microstructure of the mixing zone of  $\alpha_2/\gamma$  lamellar and  $B2$  phase is observed. So, the route of phase transformation for the Ti–46Al–8Nb in the present condition can be described as:

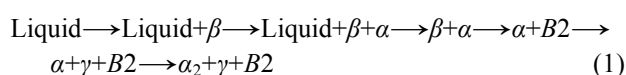
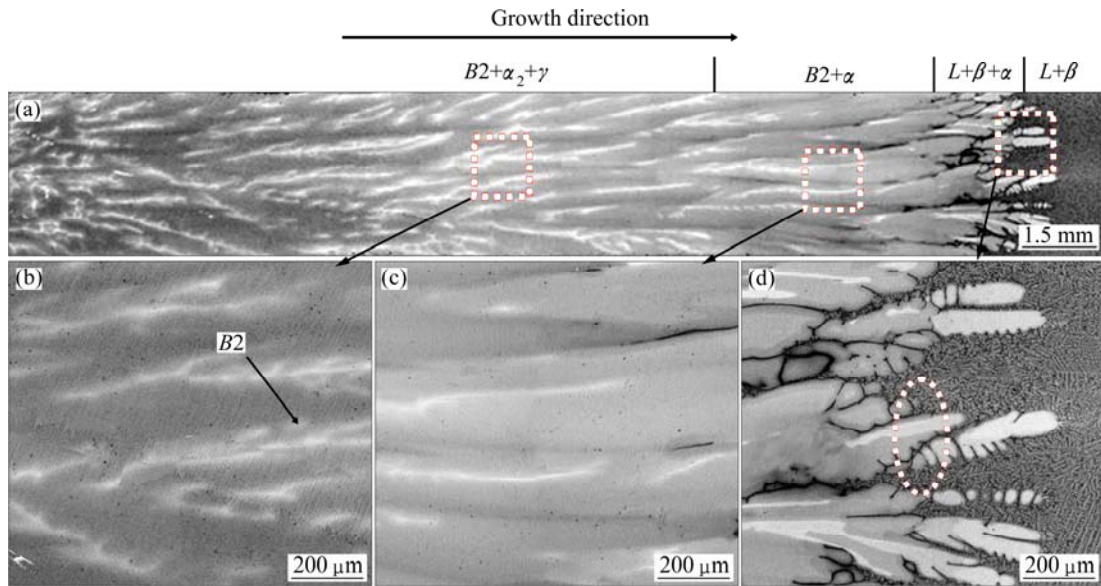
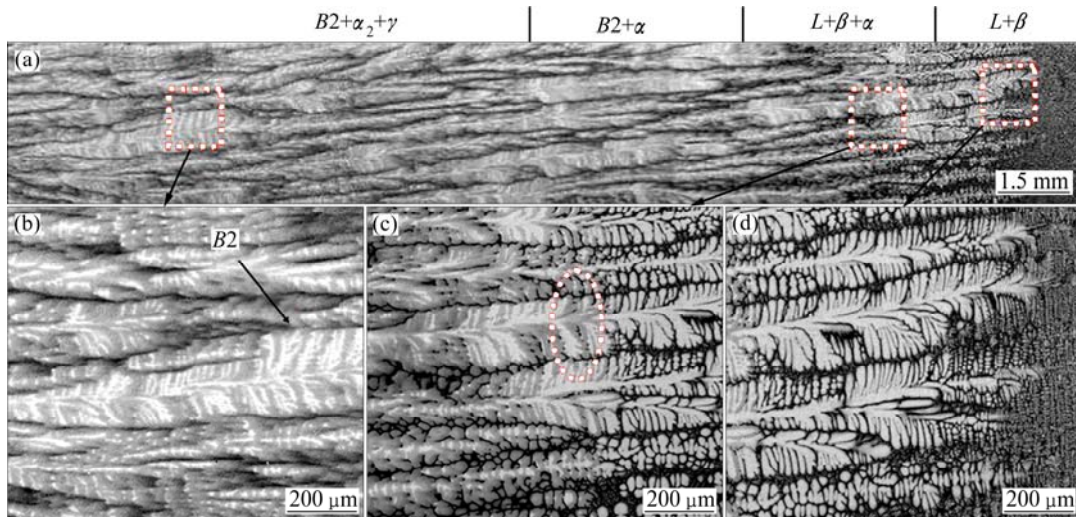


Figure 4 shows the morphologies of the quenching solid–liquid interface and the peritectic reaction interface at different growth rates. The bright contrast phase with the secondary dendritic arms orthogonal to the primary arms is identified as the primary  $\beta$  phase, and the gray regions surrounding the dendrites are found to be the peritectic  $\alpha$  phase. A regular dendritic structure is observed and the primary dendrite arm spacing decreases with the increase of growth rate. It should be noted that the change of the growth rate has a great influence on the length of solid–liquid mush zone. When the conditions of solute distribution and temperature meet the peritectic reaction, the peritectic  $\alpha$  phase can be produced as the result of the  $L+\beta$  $\rightarrow$  $\alpha$ , and the peritectic reaction interface is away from the solid–liquid interface gradually with the increase of the growth rate.



**Fig. 1** Longitudinal macrostructures (a) and microstructures (b–d) corresponding to local areas of directionally solidified Ti–46Al–8Nb alloy at growth rate of 3 μm/s



**Fig. 2** Longitudinal macrostructures (a) and microstructures (b–d) corresponding to local areas of directionally solidified Ti–46Al–8Nb alloy at growth rate of 30 μm/s

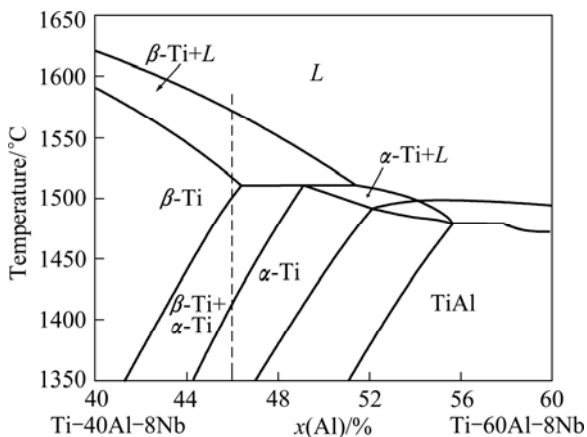


**Fig. 3** Calculated partial isopleth diagram of Ti–Al–Nb ternary system with 8% Nb [10]

Figure 5 shows the peritectic reaction occurring at different growth rates. The typical peritectic reaction is observed at 3 μm/s at the coexisted region of  $L+\alpha+\beta$ , as shown in Fig. 5(a). Peritectic phase  $\alpha$  envelops the primary phase  $\beta$  at positions behind the  $\beta$  dendrite tips in the growth direction, then grows into the former  $\beta$  dendrites through the peritectic reaction. While the peritectic phase  $\alpha$  around the secondary dendritic arms is observed at 30 μm/s, the dendrite cores represent the remaining  $\beta$  phase, as shown in Fig. 5(b). The occurrence of peritectic reaction is mainly due to the dendritic growth of primary  $\beta$  phase which leads to the solute Al discharged into the interdendritic liquid. When the enrichment of Al in the liquid satisfies the nucleation condition of peritectic  $\alpha$  phase,  $\alpha$  phase nucleates

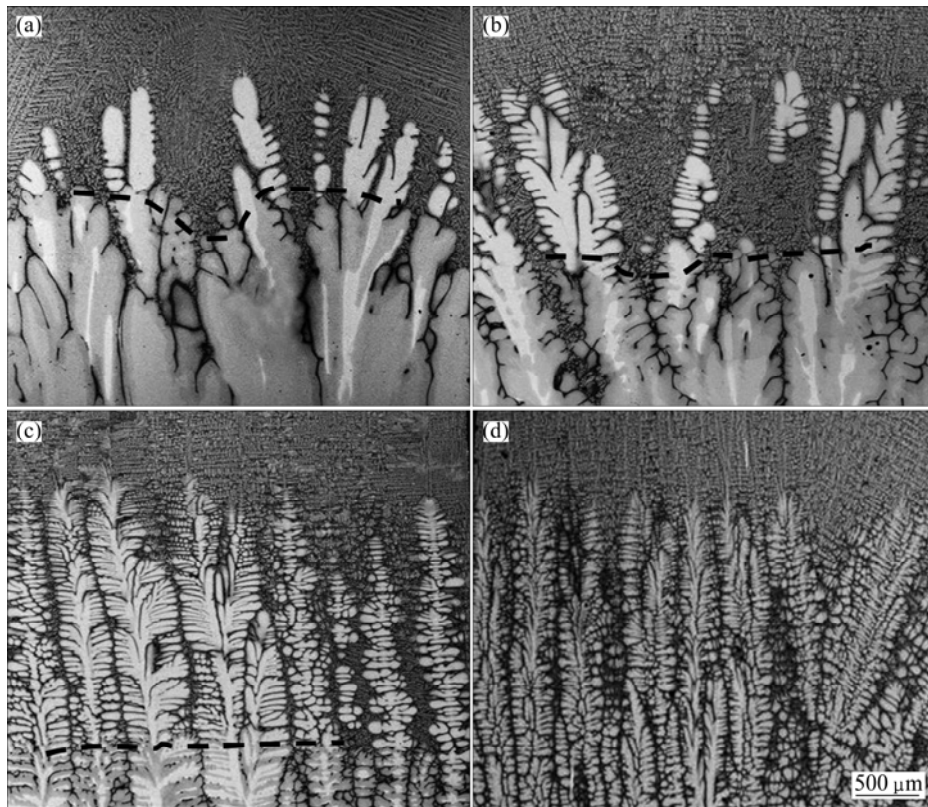


Fig. 4 Morphologies of solid–liquid interfaces at different growth rates: (a) 3  $\mu\text{m/s}$ ; (b) 5  $\mu\text{m/s}$ ; (c) 30  $\mu\text{m/s}$ ; (d) 70  $\mu\text{m/s}$

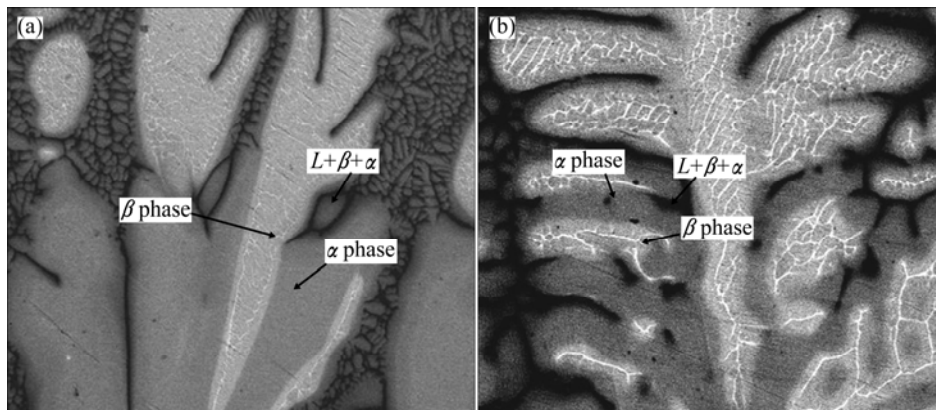
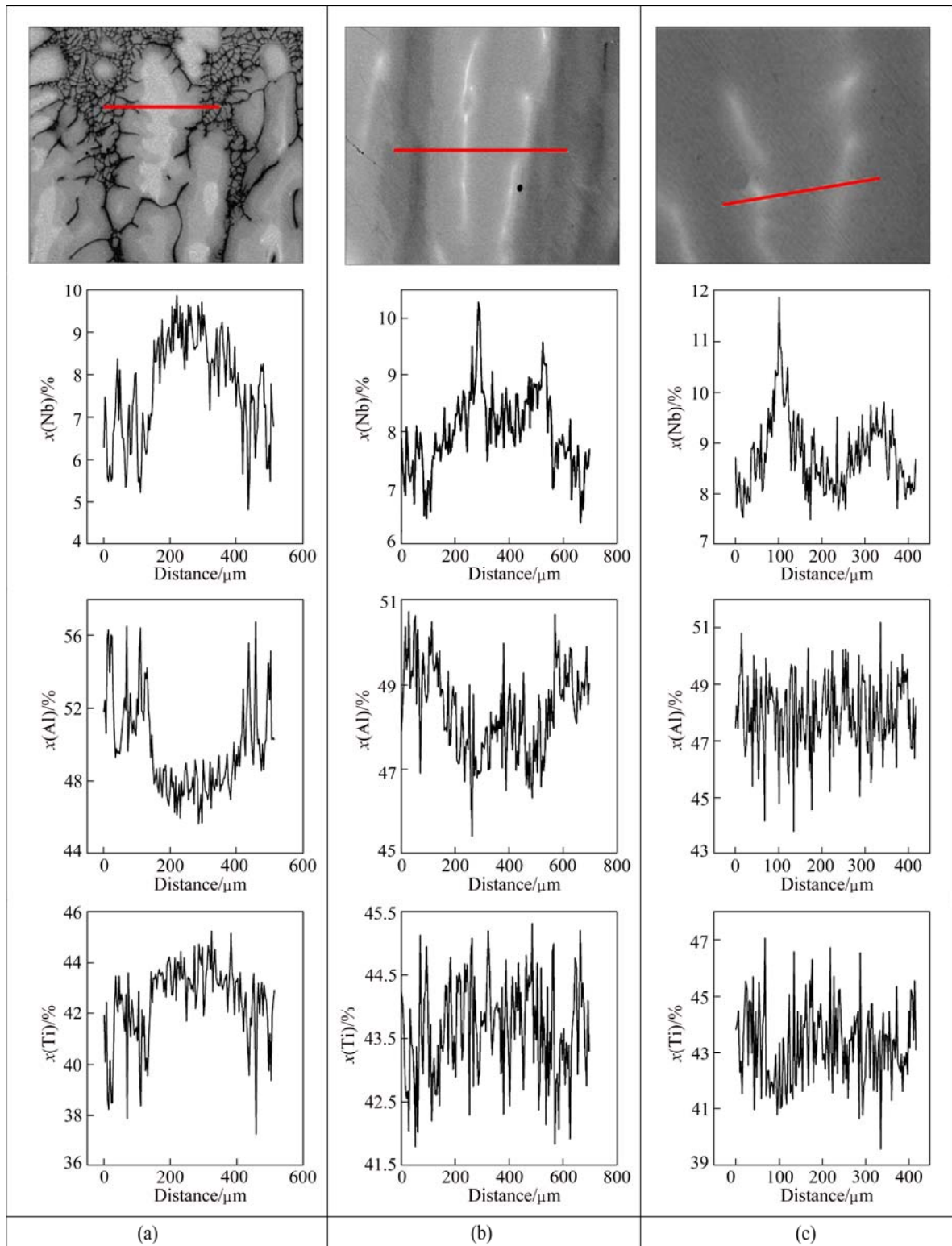


Fig. 5 Peritectic reaction morphologies at different growth rates: (a) 3  $\mu\text{m/s}$ ; (b) 30  $\mu\text{m/s}$

adhering to primary  $\beta$  dendrite. With the decrease of temperature, the growing  $\alpha$  phase envelops and dissolves the  $\beta$  phase gradually by peritectic reaction of  $L+\beta\rightarrow\alpha$ . Once the primary  $\beta$  phase is isolated from the liquid by primary  $\alpha$  phase, the sequent growth of  $\alpha$  phase needs the solute diffusion between the liquid and  $\beta$  phase by peritectic transformation whose driving force depends on the local concentrations difference of  $\alpha$  phase, i.e., the solid solubility limit. Due to the low diffusion coefficient in solid phase relative to the cooling rate, it is difficult to conduct a complete peritectic reaction. So, maintained frame of  $\beta$  dendrites can be observed clearly in Fig. 5.

### 3.2 Microsegregation and formation of B2 phase

During the directional solidification of Ti–46Al–8Nb alloy, the occurrence of peritectic reaction and subsequent solid-state transformation resulted in a complex multiphase material (B2 inter and intra granular,  $\alpha_2/\gamma$  lamellar), which may cause a significant chemical inhomogeneity and induce a scatter of mechanical properties [14–16]. So, it is important to investigate the solute distribution in the process of directional solidification of Ti–46Al–8Nb. Figure 6 shows the quantitative concentration line profiles obtained by EDS analysis in the zone of  $L+\alpha+\beta$ ,  $\alpha+\beta$  and  $\alpha_2+\gamma+B2$  at the growth rate of 5  $\mu\text{m/s}$ .



**Fig. 6** Results of EDS qualitative analyses for Ti, Al, and Nb in different zones at growth rate of 5  $\mu\text{m/s}$ : (a)  $L+\alpha+\beta$  zone; (b)  $\alpha+\beta$  zone; (c)  $\alpha_2+\gamma+B_2$  zone

In  $L+\alpha+\beta$  zone, as shown in Fig. 6(a), quantitative EDS analyses reveal that the dendrite cores are rich in Nb and depleted in Al, clearly indicating that the peritectic  $\alpha$  phase has formed in these regions. The

growth of primary  $\beta$  phase leads to the solute Al rich in the interdendritic, which promotes the occurrence of peritectic reaction. After the formation of peritectic  $\alpha$  phase in the interdendritic region,  $\alpha$  phase grows into the

former  $\beta$  dendrites through the peritectic reaction. However, due to the low diffusion coefficient in solid phase, it is difficult to conduct a complete peritectic reaction, which leads to the remaining  $\beta$  phase rich in Nb distributed in the core of dendrites.

During directional solidification, the peritectic reaction will finish when the liquid is completely solidified, and with the decrease of temperature, the solid-state phase transformation of  $\beta \rightarrow \alpha$  should take place. EDS analysis shows that the segregation amplitude of Nb rich in the core of dendrite increases rapidly, and conversely the segregation amplitude of Al decreases compared with the solute distribution in  $L+\alpha+\beta$  zone. During the transformation of  $\beta \rightarrow \alpha$ , the Al must diffuse to  $\alpha$  phase while the Nb is going in opposite direction. This tendency leads to richer in Nb in the core of the dendrite. Therefore, as the transformation continuously takes place, the Nb can be abounded in the residual  $\beta$  phase gradually, which leads to the formation of  $B2$  phase attributed to the stabilization of the residual  $\beta$  phase due to  $\beta \rightarrow \alpha$  transformation. As shown in Figs. 7(a) and (b), bright block  $B2$  phase is distributed in the core of the dendrite. With the increase of the growth rate, the volume fraction of  $B2$  phase increases gradually. At high growth rates,  $B2$  phase in a dendritic distributed is

observed owing to the greatly developed secondary dendritic arms, as shown in Figs. 7(c) and (d). In addition, the solute Al rich in the interdendritic is consumed by the growth of  $\alpha$  phase, which makes the segregation amplitude of Al decrease.

With the continuous cooling,  $\alpha$  grain could transfer to full lamellar structure of  $\alpha_2/\gamma$ . It is interesting to see that the distribution of Al becomes homogeneous gradually, and the segregation amplitude of Nb in the core of the dendrite still keeps a high level in the  $\alpha_2+\gamma+B2$  zone, as shown in Fig. 6(c). The solute distribution above reveals that the segregation of Nb increases gradually, while Al is rich in the interdendritic during the process of solidification and becomes homogeneous during the solid transformation. These can be explained as follows: The growth of  $\alpha$  phase consuming the solute Al occupies the whole of interdendritic region, leading to Al distributed homogeneously. In addition, the concentration difference between the interdendritic and the core of dendrite in solid solution  $\alpha$  phase can be as the driving force promoting the solute Al distributed homogeneously during the solid transformation. Nb can keep high segregation amplitude, which can be attributed to the diffusion ability of the atoms. As shown in Table 2, Ti

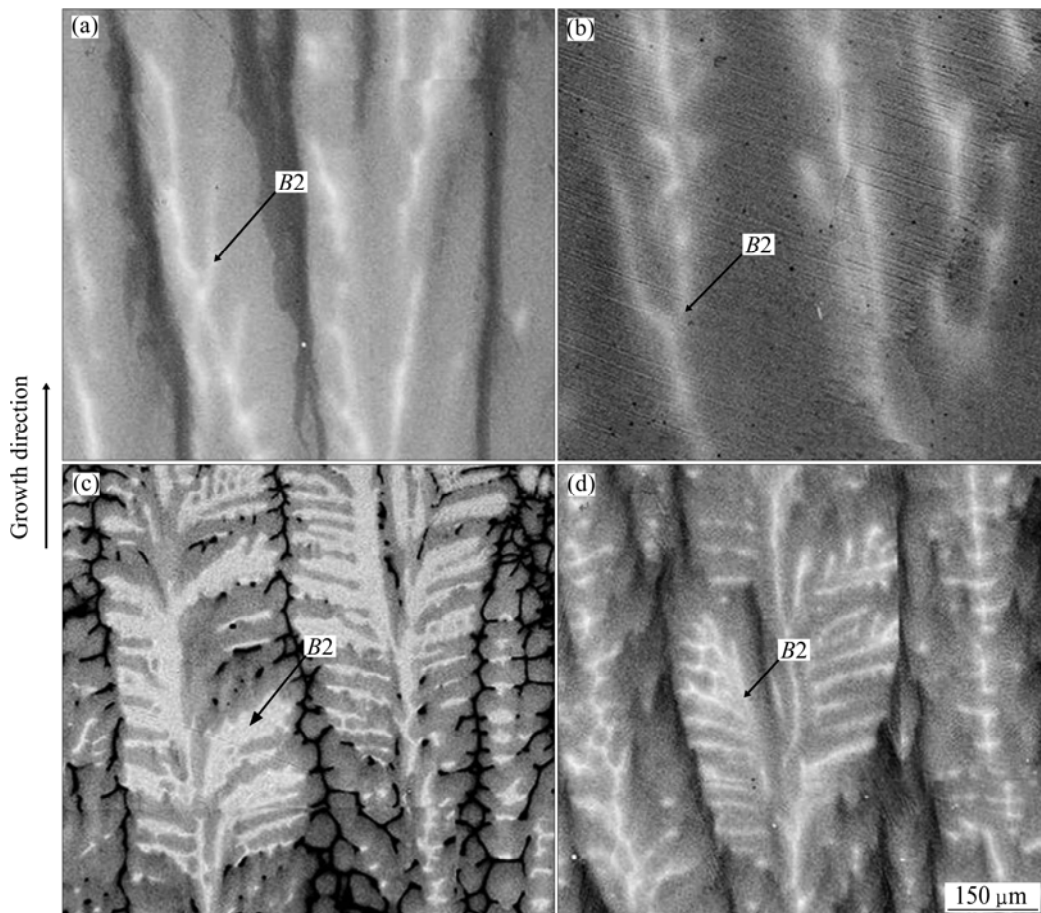


**Fig. 7** Morphologies of  $B2$  phase in different zones at different growth rates: (a) In  $\alpha+\beta$  zone at  $3 \mu\text{m/s}$ ; (b) In  $\alpha+\beta$  zone at  $30 \mu\text{m/s}$ ; (c) In  $\alpha_2+\gamma+B2$  zone at  $3 \mu\text{m/s}$ ; (d) In  $\alpha_2+\gamma+B2$  zone at  $30 \mu\text{m/s}$

and Al atoms have an identical electronegativity value of 1.5 with a corresponding atomic radius of 0.239 and 0.236 nm. Nb owns larger atomic radius and electronegativity than Ti or Al, which need to overcome bigger energy barrier during the process of the diffusion. Therefore, Nb is a slower diffuser than Ti and Al, and can keep a high segregation amplitude after directional solidification.

**Table 2** Atomic radii and electronegativities of relevant alloying elements

Element	Atomic radius/nm	Electronegativity
Ti	0.239	1.50
Al	0.236	1.50
Nb	0.243	1.60

### 3.3 Orientation of lamellar structure

The final microstructures of  $\alpha_2/\gamma$  lamellar and  $B_2$  phase are observed in directionally solidified Ti–46Al–8Nb alloy. The lamellar structure of TiAl-based alloys consists of the  $\gamma$  and  $\alpha_2$  phases with the  $(111)_\gamma // (0001)_{\alpha_2}$  relationship, and the orientation of which is determined by the primary phase. When  $\alpha$  phase is formed as the primary phase, the lamellar structure usually has the orientation perpendicular to the growth direction. While when the  $\beta$  phase is formed as the primary phase, the microstructure usually has performance with the lamellar boundaries oriented parallel and  $45^\circ$  to the growth direction [17]. By using polysynthetically twinned (PST) crystal, the mechanical properties are found to be extremely anisotropic with respect to the lamellar orientation, and the optimum combination of strength, toughness, and ductility can be obtained if the lamellar microstructure is aligned parallel to the test axis. However, PST crystal is usually extremely brittle if the lamellar structure is perpendicular to the tensile axis [18,19].

As shown in Fig. 8, it is observed that only two orientations of the lamellar structure are found in each grain. They are roughly at  $0^\circ$  or  $45^\circ$  to the primary growth direction of the  $\beta$  dendrite. The solidification usually starts with the formation of primary  $\beta$  dendrites, which often grows preferentially in  $\langle 100 \rangle$  directions parallel to the heat-flow direction. When peritectic  $\alpha$  phase is nucleated and envelops the primary  $\beta$  phase, orientation variants of  $\alpha$  phase can be inherited from the primary  $\beta$  phase by a specific orientation relationship. In all cases examined,  $\alpha$  phase of the lamellar structure is related to the  $\beta$  dendrite by the well-known Burgers relationship:  $\{110\}_\beta // (0001)_\alpha$  and  $\langle 111 \rangle_\beta // \langle 11\bar{2}0 \rangle_\alpha$ .

This results in the formation of 12 possible orientation variants of  $\alpha$  with respect to  $\beta$ . However, under solidification conditions where a steep temperature

gradient exists, only a single variant of the 12 variants may appear. It is found that  $\alpha$  phase grows through  $\beta$  dendrites in such a way. Thus, the orientation of lamellar structure is determined, relative to the pre-existing  $\beta$  phase.

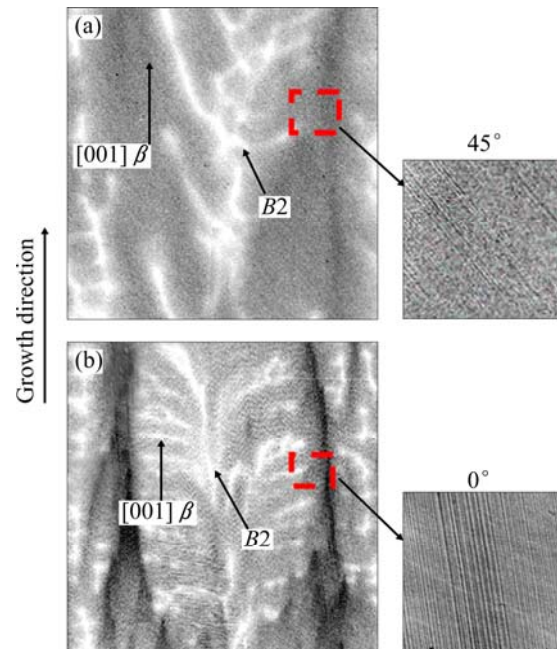


**Fig. 8** Different orientation relationships of lamellar: (a) Lamellar interface at about  $45^\circ$  to primary arms at growth rate of  $3 \mu\text{m/s}$ ; (b) Lamellar interface at about  $0^\circ$  to primary arms at growth rate of  $30 \mu\text{m/s}$

## 4 Conclusions

1) In the range of growth rate of  $3\text{--}70 \mu\text{m/s}$ , a regular dendritic structure appears, and the primary dendrite arm spacing decreases with the increase of growth rate. The peritectic reaction was observed in DS samples. After directional solidification, the final microstructure is composed of  $\alpha_2/\gamma$  lamellar structures and retaining  $\beta(B_2)$  phase.

2) Peritectic solidification leads to a significant chemical inhomogeneity, in which aluminum is rich in the interdendrite and niobium is rich in the core of the dendrite during the solidification process. With the nucleation and growth of  $\alpha$  phase, the segregation amplitude of niobium increases, while aluminum rich in the interdendritic becomes homogeneous gradually.

3)  $B_2$  phase with a light block shape distributes in the core of the dendrite due to the  $\beta \rightarrow \alpha$  transformation. With the increase of the growth rate, the  $B_2$  phase is in a dendrite distribution owing to the greatly developed secondary dendritic arms. The volume fraction of  $B_2$  phase increases with the increase of the growth rate.

4) The  $\alpha_2/\gamma$  lamellar only lies parallel and  $45^\circ$  to the growth direction by the Burgers orientation relationship

under a strong temperature gradient. The orientation of lamellar structure is determined by the pre-existing  $\beta$  phase.

## References

- [1] ZHENG Zhi, JIANG Yao, DONG Hong-xing, TANG Lie-min, HE Yue-hui, HUANG Bai-yun. Environmental corrosion resistance of porous TiAl intermetallic compounds [J]. Transactions of Nonferrous Metals Society of China, 2009, 19(3): 581–585.
- [2] HUANG S C, SHIH D S. Microstructure-property correlation in TiAl-base alloys [M]. Warrendale, PA: TMS, 1991: 105.
- [3] XIAO Shu-long, TIAN Jing, XU Li-juan, CHEN Yu-yong, YU Hong-bao. Microstructures and mechanical properties of TiAl alloy prepared by spark plasma sintering [J]. Transactions of Nonferrous Metals Society of China, 2009, 19(6): 1423–1427.
- [4] LIU Z C, LIN J P, LI S J, CHEN G L. Effects of Nb and Al on the microstructures and mechanical properties of high Nb containing TiAl base alloys [J]. Intermetallics, 2002, 10(7): 653–659.
- [5] DIMIDUK D M. Gamma titanium aluminide alloys—An assessment within the competition of aerospace structural materials [J]. Materials Science and Engineering A, 1999, 263: 281–288.
- [6] LIU C T, SCHNEIBEL J H, MAZIAX P J, WRIGHT J L, EASTON D S. Tensile properties and fracture toughness of TiAl alloys with controlled microstructures [J]. Intermetallics, 1996, 4(6): 429–440.
- [7] TAKEYAMA M O H, MURA Y, KIKUCHI M, MATSUO T. Phase equilibria and microstructural control of gamma TiAl based alloys [J]. Intermetallics, 1998, 6: 643–646.
- [8] YOSHIHARA M, MIURA K. Effects of Nb addition on oxidation behavior of TiAl [J]. Intermetallics, 1995, 3(5): 357–363.
- [9] JARVIS D J, VOSS D. IMPRESS integrated project—An overview paper [J]. Materials Science and Engineering A, 2005, 413–414: 583–591.
- [10] KARTAVYKHA A., GINKINB V, GANINAB S, REXC S, HECHTC U, SCHMITZD B, VOSSE D. Convection-induced peritectic macro-segregation proceeding at the directional solidification of Ti-46Al-8Nb intermetallic alloy [J]. Materials Chemistry and Physics, 2011, 1–2: 200–206.
- [11] NAKAMURA H, TAKEYMA M, YAMABE Y, KIKUCHI M. Phase equilibria in TiAl alloys containing 10 and 20 at% Nb at 1473 K [J]. Scripta Metallurgica et Materialia, 1993, 28: 997.
- [12] LEONARD K J, VASUDEVAN V K. Phase equilibria and solid state transformations in Nb-rich Nb-Ti-Al intermetallic alloys [J]. Intermetallic, 2000, 8 (9–11): 1257–1268.
- [13] DING X F, LIN J P, ZHANG L Q, WANG H L, HAO G J, CHEN G L. Microstructure development during directional solidification of Ti-45Al-8Nb alloy [J]. Journal of Alloys and Compounds, 2010, 506(1): 115–119.
- [14] ZOLLINGER J, DALOZ D, COMBEAU H, LAPIN J. Microstructures and microsegregation formation in TiAl-based alloys containing niobium [C]// Proceedings of the 5th Decennial International Conference on Solidification Processing. Sheffield, 2007.
- [15] IMAVEY R M, IMAYEV V M, OEHRING M, APPEL F. Alloy design concepts for refined gamma titanium aluminide based alloys [J]. Intermetallics, 2007, 15(4): 451–460.
- [16] DIMIDUK D M, MARTIN P L. Microstructure development in gamma alloy mill products by thermomechanical processing [J]. Materials Science and Engineering A, 1998, 243(1–2): 66–76.
- [17] YAMAGUCHI M, JOHNSON D R, LEE H N, INUI H. Directional solidification of TiAl-base alloys [J]. Intermetallics, 2000, 8: 511–517.
- [18] JOHNSON D R, CHIHARA J K, INUI H, YAMAGUCHI M. Microstructural control of TiAl-Mo-B alloys by directional solidification [J]. Acta Materialia, 1998, 46(18): 6529–6540.
- [19] UMSKOSHIA Y, NAKANO T, YAMANE T. The effect of orientation and lamellar structure on the plastic behavior of TiAl crystals [J]. Materials Science and Engineering A, 1992, 152(1–2): 81–88.

# 定向凝固 Ti-46Al-8Nb 合金的 微观组织演变与微观偏析

刘国怀, 李新中, 苏彦庆, 陈瑞润, 郭景杰, 傅恒志

哈尔滨工业大学 材料科学与工程学院, 哈尔滨 150001

**摘要:** 在 3~70  $\mu\text{m/s}$  的生长速度范围内对 Ti-46Al-8Nb (摩尔分数, %)合金进行定向凝固实验, 研究其微观组织演变和微观偏析形式。在该生长速度范围内, 固-液界面表现为规则的枝晶生长, 一次枝晶间距随着生长速度的加快而逐渐减小。在定向凝固过程中观察到典型的  $L+\beta \rightarrow \alpha$  包晶反应, 最终得到具有  $\alpha_2/\gamma$  层片和 B2 相的微观组织。在各个晶粒中, 层片与  $\beta$  相枝晶初始生长方向呈  $0^\circ$  或  $45^\circ$ 。包晶反应导致严重的成分偏析, 在凝固过程中, 铝富集在枝晶间, 铌富集在枝晶心部。随着  $\alpha$  相的形核和生长, 铌的偏析程度逐渐增大, 从而促进 B2 相的析出, 而富集在枝晶间的铝在包晶反应发生后逐渐变得均匀、一致。

**关键词:** Ti-46Al-8Nb 合金; 定向凝固; 组织演变; 微观偏析; 层片取向

(Edited by LI Xiang-qun)